An artificial sensory neuron with tactile perceptual learning

Wan, Changjin; Chen, Geng; Fu, Yangming; Wang, Ming; Matsuhisa, Naoji; Pan, Shaowu; Pan, Liang; Yang, Hui; Wan, Qing; Zhu, Liqiang; Chen, Xiaodong

2018

Wan, C., Chen, G., Fu, Y., Wang, M., Matsuhisa, N., Pan, S., . . ., Chen, X. (2018). An artificial sensory neuron with tactile perceptual learning. Advanced materials, 30(30), 1801291-. doi:10.1002/adma.201801291

https://hdl.handle.net/10356/137788

https://doi.org/10.1002/adma.201801291

DOI: 10.1002/(adma.201801291)
Article type: Communication

An Artificial Sensory Neuron with Tactile Perceptual Learning

Changjin Wan, Geng Chen, Yangming Fu, Ming Wang, Naoji Matsuhisa, Shaowu Pan, Liang Pan, Hui Yang, Qing Wan, Liqiang Zhu, & Xiaodong Chen **

Dr. C. Wan, G. Chen, Dr. M. Wang, Dr. N. Matsuhisa, Dr. S. Pan, Dr. L. Pan, Dr. H. Yang, Prof. X. Chen
Innovative Center for Flexible Devices (iFLEX), School of Materials Science and Engineering Nanyang Technological University, 50 Nanyang Avenue 639798, Singapore.
E-mail: chenxd@ntu.edu.sg

Y. Fu, Prof. L. Zhu
Key Laboratory of Graphene Technologies and Applications of Zhejiang Province, Ningbo Institute of Materials Technology and Engineering, Chinese Academy of Sciences, Ningbo 315201, Zhejiang, People's Republic of China
E-mail: lqzhu@nimte.ac.cn

Prof. Q. Wan
School of Electronic Science & Engineering, Nanjing University, Nanjing 210093, Jiangsu, Peoples Republic of China

Keywords: artificial neuron, perceptual learning, artificial intelligence, electronic skin, neuromorphic engineering

Abstract

Sensory neurons within skin form an interface between the external physical reality and the inner tactile perception. This interface enables us to organize, identify and interpret the sensory information through perceptual learning—the process whereby our sensing abilities improves through experience. Here, we show an artificial sensory neuron that could integrate and differentiate the spatiotemporal features of touched patterns for recognition. The system comprises sensing, transmitting and processing components that are parallel to those found in a sensory neuron. A resistive pressure sensor converts pressure stimuli into electric signals, which are transmitted to a synaptic transistor through interfacial ionic/electronic coupling via a soft ionic conductor. Furthermore, the recognition error rate could be dramatically decreased from 44% to 0.4% by integrating with the machine learning method. This work

represents a step toward the design and use of neuromorphic electronic skin with artificial intelligence for robotics and prosthetics.

Tactile perception relies on comprehensive activities of sensing, refining and learning, which enormously shapes our interactions with the external environment. [1, 2] Physiologically, touch is detected by receptors on sensory neurons embedded in the skin. Signals are sent along a long chain of afferent axons to synapses for postsynaptic neurons to further process. [3, 4] Neurons integrate and modulate both synchronous and asynchronous tactile stimuli to obtain multilevel features of the touch in an action-perception loop (**Figure 1**a), which underlies the tactual perception. Through practice and/or training, tactile perception could be further enhanced with learned expertise, which empowers us to perceive precisely and react appropriately to the events of the real world.[5, 6] Therefore, endowing robots and prosthesis with such perceptual learning capability could potentially extend their cognition and adaptability.[7-10] To achieve this, there is a need for the creation of artificial sensory neuron with perceptual learning.

The integration of sensing and processing components has been proposed for capturing similarities of sensory neuron.[11-14] For example, haptic memory was realized in a device that integrates resistive switching memory with resistive pressure sensors. [11] Although such design allows touch information to be retained after the stimuli are removed, it cannot directly differentiate tactile patterns. A more recent device consisting of a transistor-based pressure sensor and an electrolyte gated synaptic transistor was proposed to filter touch rate.[12] While such device is able to differentiate tactile patterns, it lacks learning capabilities necessary for identification and recognition tasks. Therefore, to implement learning within device/system level is very required for robust and fault-tolerant processing of tactile stimuli. Furthermore, the addition of learning capability would ultimately provide machines or systems with artificial intelligence that enables them to replicate 'cognitive' functions of the human.[15, 16]

Here, we show a neuromorphic tactile processing system (NeuTap) that mimics the sensory neuron and is capable of perceptual learning. In our design, the receptor that senses,

axon that transmits and synapse that processes information in a sensory neuron is represented by a resistive pressure sensor, a soft ionic cable and a synaptic transistor, respectively (Figure 1b). The pressure sensor converts pressure stimuli into electrical signals, which are transmitted by interfacial ion/electron coupling to the synaptic transistor via an ionic cable. The synaptic transistors then induce specific decay properties corresponding to the stimuli patterns. In addition, our design provides an event-driven approach that utilizes external touch to activate the synaptic devices. [17-19] As a proof-of-concept, we demonstrate that the NeuTap is capable of recognizing tactile patterns by extracting the spatiotemporal correlated tactile feature, and we improve the recognition capability by implementing perceptual learning in the systems.

Our NeuTap prototype resembles the biological sensory neuron in that the sensing and processing components are separated by the soft ionic cable. This separation could be benefit for suppression of interferences between the two components and confers flexibility to the system as well. [20] The detailed schematic diagrams are shown in Figure 1c. The resistive pressure sensor [21, 22] consists of two layers (Figure 1c): the top one composing the pressure sensitive layer, which is pyramidal poly (dimethylsiloxane) (PDMS) coated with carbon nanotubes (CNTs); and the bottom one composing polyethylene terephthalate (PET) with gold interdigital electrodes for detecting resistance change (Figure S1 and Figure S2, Supporting Information). **Figure 2**a shows resistance change of a sensor responding to different applied pressures where resistance drops significantly and the sensitivity shows a gradual decay when additional external pressures are applied at very low regimes (0.1-1 kPa). [11, 23] The ionic cable [20, 24, 25] comprises of two ionic conducting polyvinyl alcohol (PVA) wires that are connected to two terminals of the interdigital electrodes on the pressure sensor (Figure S3, Supporting Information). PVA possess high fracture strain and good ionic conductivity, [26, 27] which is suitable for soft ionic conducting wires (Figure S4, Supporting Information). PDMS was used as both insulation and encapsulation materials for the PVA-based ionic cable. The

Cole-Cole plot of the PVA layer seen in Figure 2b shows a perfect semi-circle, suggesting an ideal Debye type behavior. [27, 28] We estimated the ionic conductivity of the PVA layer to be 3×10^{-3} S cm^{-1} (Figure S5 and Figure S6, Supporting Information). What's more, the ionic cable retains good conductivity even under a strain up to ~40% (Figure S7 and Figure S8, Supporting Information). On the synaptic transistor side, one PVA wire contacts a gold electrode (V_{DD}) to supply voltage, and the other PVA wire is covered on the indium-tungsten-oxide (IWO) channel and serves as a gate dielectric (Figure S9 and Figure S10, Supporting Information). Figure 2c shows the transfer curves of the PVA gated IWO transistor for five times indicating typical field-effect transistor performance. The sweep rate of V_{GS} is 0.05 V/s and the sampling frequency is 1 Hz. Low leakage current of <10 nA is achieved, illustrating good insulating property of the PVA gate dielectric.

To show that neuromorphic behaviors could be implemented using the PVA gated IWO transistors, some short-term plasticity emulations were achieved (Figure S11, Supporting Information), and the paired pulse facilitation (PPF) emulation [17, 29, 30] were shown as an example (Figure 2d). In the experiment, when two successive voltage pulses (-1.5 V, 10 ms) with a time interval (ΔT) of 200 ms was applied on the gate, two current peaks were observed and the amplitude of the second one (A_2) is ~1.25 times higher than that of the first one (A_1). The facilitation ratio (A_2/A_1), decreases with the increasing of pulse-to-pulse interval (ΔT) (inset of Figure 2d), indicating a PPF phenomenon.

In the NeuTap, a voltage (V) applied on V_{DD} leads to a voltage drop in the PVA wires, the pressure sensor and the semiconducting channel. When no pressure is applied on the sensor, the resistance of the sensor is extremely large and the voltage drop on the sensor is almost equal to V. When the sensor is pressed, resistance decreases dramatically and this increases the voltage drop across the PVA wires. Such an abrupt increase in voltage drop is similar to applying a voltage pulse on the PVA ionic conducting wires, which would trigger ionic fluxes. Due to the electric-double-layer (EDL) effect, accumulation of ions at the

IWO/PVA interface induces a strong electric-field intensity,[31, 32] which accordingly tunes the conductance of the IWO channel. During the press, more and more ions accumulate at the interface and this aggravates the variation trend of the channel conductance. Because the IWO is an n-type semiconductor, negative (positive) V_{DD} would result in a decrease (increase) in conductance. When the sensor is released, voltage drop applied on the PVA will decrease suddenly. However, the ions in the PVA partially remain near the interface before gradually drifting back to their equilibrium position. Therefore, the channel conductance decays back to its initial value gradually. The change in conductance during the touch is similar to the memory process, while recovery in conductance after touch is analogous to the forgetting process. Previous synaptic devices possess similar memory/forgetting behaviours.[33-36] However, the changes in dynamic conductance in these devices are achieved by programmed voltage pulses. Our design provides an event-driven approach that utilizes external touch to activate the synaptic devices.

Tactual perception begins with the complex integration of multiple spatiotemporal correlated sensory stimuli. This process allows us to recognize objects, discriminate texture, and react appropriately in a social exchange. [2, 3] Two processes shown in **Figure 3**a and 3b, respectively, were mimicked to demonstrate our devices are capable for such spatiotemporal integration. [37, 38] In the first case, two isolated stimulations were triggered synchronously, and both could excite the sensory neuron (Figure 3a). Such a process would augment the neuronal response more effectively than applying a single stimulation. This process resembles a situation where the touch of two fingers at once brings greater sensation and awareness to an individual than the touch of one finger at the same pressure value. In the second case, two stimulations were triggered asynchronously, where the first stimulation excited and the second one inhibited the sensory neuron (Figure 3b). This case resembles a situation where pain is alleviated by gentle strokes.

To mimic these cases, we fabricated NeuTap with two pressure sensing terminals (Figure 3c). Each of the pressure sensors has an individual voltage source labelled as V_{DD1} and V_{DD2}, respectively. Therefore, if either of the sensors was loaded with a pressure, the voltage applied on the sensor would be coupled to the IWO channel through the PVA based ionic conductor. As shown in Figure 3d, when sensor 1 is loaded with a 1 kPa pressure, a metal-insulator-transition with ON/OFF ratio of ~10^5 (orange curve) could be observed when the voltage of V_{DD1} sweeps from -2.0 to 1.0 V. However, when sensor 2 is also loaded with a 1 kPa pressure, the drain current (I_{DS}) will be suppressed or augmented at most of the V_{DD1} sweep range by a negative (-1.0 V) or positive (1.0 V) V_{DD2}, respectively. In other words, the channel conductance could be tuned by the joint effect from the two sensors. As shown in Figure 3e, when both V_{DD1} and V_{DD2} are -1.0 V, we first pressed the two sensors individually by finger and then pressed the two sensors simultaneously. The responses of the synaptic transistor were nearly identical when the sensors were pressed individually (blue and green curves). However, the response to the simultaneous stimuli nearly doubled in logarithmic scale. These results indicate that the NeuTap could concurrently integrate spatially isolated tactile stimuli, which is very similar to the case described in Figure 3a. Next, when V_{DD1} is -1.0 V and V_{DD2} is 0.5 V, we first pressed sensor 1 followed by sensor 2 as shown in Figure 3f. Upon pressing sensor 1, current decreases dramatically. By repeatedly pressing sensor 2, the current could be tuned stepwise back to the initial level. These results indicate that the NeuTap could also integrate the spatiotemporal correlated tactile stimuli, which is very similar to the case described in Figure 3b.

Next, as a proof-of-concept, we used the NeuTap neuron with one sensing terminal to implement tactile pattern recognition. Two patterns in one row were used as the object for recognition (**Figure 4**a). To label all the pattern pairs, we defined the convex pattern in the pair as ‘1’ and the flat pattern as ‘0’. Therefore, each pattern pair was labelled using a binary code as follows: ‘00’, ‘01’, ‘10’ and ‘11’, respectively. In the experiment, the NeuTap was

attached to a finger, and the finger was brought close to the patterns and moved from left to right. A complete move-touch action takes ~5s (T_R=5 s, where T_R is defined as the time when the touch is just ended). The conductance of the transistor channel was measured as output in each experiment. Only pattern '1' would induce a pressure change and result in a conductance change through the IWO channel. Obvious differences could be seen among the responses of the nonzero-labeled ('10', '01' and '11') patterns (Figure 4b). The '11' pattern showed the largest change in conductance (ΔG) because this pattern could provide two successive pressure stimuli. Although both '01' and '10' patterns have only one convex pattern, the timing information of the two patterns is different. The response to the '10' pattern decays earlier than the response to the '01' pattern. Therefore, the conductance response to the '01' pattern is higher than the '10' pattern after the move-touch action ($t>T_R$). Because the responses to the pattern pairs after each action are distinguishable, these responses could be used as the specific features for recognition. To mimic the perceptual learning process, supervised learning method was implemented in NeuTap (Figure 4c). Supervised learning is widely used for pattern classification and numerical regression, [15, 39] which analyzes the input object and desired value (the pair is named as training data) to generate an inferred function for mapping new examples. We first defined the relative change in channel conductance after an action ($t>T_R$) as the recognition index (RI):

$$RI(\mathrm{t}) = \frac{\Delta G(\mathrm{t})}{G_0}, t > T_R \qquad (1)$$

where $\Delta G_i(t)$ is the changes in conductance after a touch and G_0 is the initial value of the conductance. Several groups of RI data for the three pattern pairs were obtained through replicate measurements. These RI data and their corresponding labels served as the training data. These data were fed into the computer program to divide the boundaries for each pattern. When unlabeled RI data (the testing data; RI' in Figure 4c) were input, the computer compares the RI' values with 'learned' boundaries and inferred the labels of the patterns.

The RI data for each of the three nonzero-label pattern pairs and their corresponding labels are shown in Figure 4d. Each pattern was measured four times, and these data were served as the training dataset. Then the boundaries for classification could be determined (green dash-dot lines in Figure 4d and Figure S12 in Supporting Information) based on this dataset. In this work, we use the k-nearest neighbours (KNN) algorithm for calculation (Note S1, Supporting Information). We also defined the boundary for '00' pattern as RI=10%. Therefore, the RI data at each time point could be divided by the boundaries (the green dash-dot line) into four regions as '11', '01', '10' and '00', respectively. Although the *RI* data of each given pattern pairs show a similar trend, a certain level of variation could be clearly observed. This variation is likely due to the inevitable differences in the applied pressure and the speed of the finger when moving across the pattern pairs (Figure S13, Supporting Information). In principle, due to the memory effect of the synaptic element, the recognition could be executed at any time before the RI for all the pattern decays to 0% showing no difference to each other. The testing time in this work is uniformly set to 20 s and the recognition thus could be executed within the timeframe of ~15 s (after a move-touch action) by comparing the RI data and learned boundaries at any time point.

Conductance data in Figure 4b were used as an example testing dataset to test the recognition capability (Figure S14, Supporting Information). Such results show that the boundaries are valid and can be used to recognize unlabeled data even several seconds later after the move-touch action, which enable the robot's 'brain' for priority processing of more emergent and vital tasks. However, the 'learned boundaries' is not always inerrancy for a new recognition task. A certain level of variation is existed among the outputs in response to the same pattern pairs, which could bring about misjudgment by comparing with previous learned boundaries. For example, ~44% error rate could be observed for one time learning as shown in Figure 4e. The learned boundaries were obtained based on only one training dataset, and such boundaries were test by a new dataset. The misjudged points are counted by

comparing the learned boundaries and the new dataset at each time point. Then the error rate is calculated by the ratio of misjudged points. Our results in Figure 4e show a gradually decay tendency of the error rate by increasing the learning times, and a very low error rate of ~0.4% is achieved for 6 times of learning (the detailed data is available in Figure S15, Supporting Information). The range of the output variations tend to be more stable and the boundaries thus could be more accurate after several times of training. Therefore, the recognition capability by NeuTap could be enhanced through repeated training, which is similar to the perceptual learning process. Because the surface of a given object may consist of various combinations of flat and convex patterns, this method could be used to recognize more complex patterns such as braille codes (Table S1, Supporting Information)).

In summary, our NeuTap neuron, composing of the resistive pressure sensor, ionic cable, and synaptic transistor, captures essential morphological and functional similarities to biological sensory neuron. Our NeuTap neuron can integrate and modulate spatiotemporal correlated tactile stimuli, enabling parallel sensory signal processing. The features of tactile patterns thus could be integrated and extracted by such system for pattern recognition. More importantly, the recognition accuracy could be improved through repeated training, illustrating a great similarity to the perceptual learning processes. This system is potentially integrated with neuromorphic networks for complex recognition/decision that serve as guidance for the brain-machine interfaces. Furthermore, the addition of the parallel computing nature rendered by the neuromorphic component could be advantageous in integration of multiple sensory feedbacks (e. g. sight and proprioception) to profoundly promote robotic prostheses sophistication.

Experimental Section

Electrical characterizations. For pressure sensor, pressure was applied and measured by a motorized vertical test stand (Mark-10 ESM301) in combination with a force gauge (Mark-10

M5–2). The impedance measurements of PVA films were characterized by a Solartron 1260A Impedance/Gain-Phase Analyzer. The electrical measurements of the transistors and the tactile pattern recognition were performed on a semiconductor parameter characterization system (Keithley 4200 SCS) in a shielded dark box at room temperature. Other experimental details can be found in the Supporting Information.

Supporting Information
Supporting Information is available from the Wiley Online Library or from the author.

Acknowledgements
We thank the financial support from the National Research Foundation, Prime Minister's office, Singapore, under its NRF Investigatorship (NRF2016NRF-NRF1001-21) and Singapore Ministry of Education (MOE2017-T2-2-107).

Received: ((will be filled in by the editorial staff))
Revised: ((will be filled in by the editorial staff))
Published online: ((will be filled in by the editorial staff))

References

[1] R. S. Dahiya, G. Metta, M. Valle, G. Sandini, *IEEE T. Robot.* **2010**, *26*, 1.

[2] A. M. Fernandes, P. B. Albuquerque, *Cogn. Process.* **2012**, *13*, 285.

[3] V. E. Abraira, D. D. Ginty, *Neuron* **2013**, *79*, 618.

[4] E. A. Lumpkin, M. J. Caterina, *Nature* **2007**, *445*, 858.

[5] W. R. Garner, *Science* **1970**, *168*, 958.

[6] D. Y. Little, F. T. Sommer, *Front Neural Circuits* **2013**, *7*, 1.

[7] B. C.-K. Tee, A. Chortos, A. Berndt, A. K. Nguyen, A. Tom, A. McGuire, Z. C. Lin, K. Tien, W.-G. Bae, H. Wang, P. Mei, H.-H. Chou, B. Cui, K. Deisseroth, T. N. Ng, Z. Bao, *Science* **2015**, *350*, 313.

[8] K. E. Foley, *Nat Med* **2016**, *22*, 2.

[9] H. P. Saal, S. J. Bensmaia, *Neuropsychologia* **2015**, *79*, 344.

[10] C. Bartolozzi, L. Natale, F. Nori, G. Metta, *Nat. Mater.* **2016**, *15*, 921.

[11] B. Zhu, H. Wang, Y. Liu, D. Qi, Z. Liu, H. Wang, J. Yu, M. Sherburne, Z. Wang, X. Chen, *Adv. Mater.* **2016**, *28*, 1559.

[12] Y. Zang, H. Shen, D. Huang, C. A. Di, D. Zhu, *Adv. Mater.* **2017**, *29*, 1606088.

[13] H. H. Chou, A. Nguyen, A. Chortos, J. W. To, C. Lu, J. Mei, T. Kurosawa, W. G. Bae, J. B. Tok, Z. Bao, *Nat Commun* **2015**, *6*, 8011.

[14] R. A. Nawrocki, N. Matsuhisa, T. Yokota, T. Someya, *Adv. Electron. Mater.* **2016**, *2*, 1500452.

[15] P. Langley, *Machine Learning* **2011**, *82*, 275.

[16] M. I. Jordan, T. M. Mitchell, *Science* **2015**, *349*, 255.

[17] Z. Wang, S. Joshi, S. E. Savel'ev, H. Jiang, R. Midya, P. Lin, M. Hu, N. Ge, J. P. Strachan, Z. Li, Q. Wu, M. Barnell, G.-L. Li, H. L. Xin, R. S. Williams, Q. Xia, J. J. Yang, *Nat. Mater.* **2017**, *16*, 101.

[18] P. Gkoupidenis, D. A. Koutsouras, G. G. Malliaras, *Nat. Commun.* **2017**, *8*, 15448.

[19] M. Lee, W. Lee, S. Choi, J. W. Jo, J. Kim, S. K. Park, Y. H. Kim, *Adv. Mater.* **2017**, *29*, 1700951.

[20] C. H. Yang, B. Chen, J. J. Lu, J. H. Yang, J. Zhou, Y. M. Chen, Z. Suo, *Extreme Mech. Lett.* **2015**, *3*, 59.

[21] S. Gong, W. Schwalb, Y. Wang, Y. Chen, Y. Tang, J. Si, B. Shirinzadeh, W. Cheng, *Nat. Commun.* **2014**, *5*, 3132.

[22] N. N. Jason, M. D. Ho, W. Cheng, *J. Mater. Chem C* **2017**, *5*, 5845.

[23] K. K. Kim, S. Hong, H. M. Cho, J. Lee, Y. D. Suh, J. Ham, S. H. Ko, *Nano Lett.* **2015**, *15*, 5240.

[24] C. Keplinger, J.-Y. Sun, C. C. Foo, P. Rothemund, G. M. Whitesides, Z. Suo, *Science* **2013**, *341*, 984.

[25] C. H. Yang, B. Chen, J. Zhou, Y. M. Chen, Z. Suo, *Adv. Mater.* **2016**, *28*, 4480.

[26] C. Zhao, C. Wang, Z. Yue, K. Shu, G. G. Wallace, *ACS Appl. Mater. Inter.* **2013**, *5*, 9008.

[27] Z. Niu, H. Dong, B. Zhu, J. Li, H. H. Hng, W. Zhou, X. Chen, S. Xie, *Adv. Mater.* **2013**, *25*, 1058.

[28] K. S. Hemalatha, G. Sriprakash, M. V. N. A. Prasad, R. Damle, K. Rukmani, *J. Appl. Phys.* **2015**, *118*, 154103.

[29] C. Wan, L. Zhu, Y. Liu, Y. Shi, Q. Wan, *IEEE Electron Dev. Lett.* **2014**, *35*, 672.

[30] L. Q. Zhu, C. J. Wan, L. Q. Guo, Y. Shi, Q. Wan, *Nat. Commun.* **2014**, *5*, 3158.

[31] J. Jiang, J. Guo, X. Wan, Y. Yang, H. Xie, D. Niu, J. Yang, J. He, Y. Gao, Q. Wan, *Small* **2017**, *13*, 1700933.

[32] W. Xie, X. Zhang, C. Leighton, C. D. Frisbie, *Adv. Electron. Mater.* **2017**, *3*, 1600369.

[33] T. Chang, S. H. Jo, W. Lu, *ACS Nano* **2011**, *5*, 7669.

[34] T. Ohno, T. Hasegawa, T. Tsuruoka, K. Terabe, J. K. Gimzewski, M. Aono, *Nat. Mater.* **2011**, *10*, 591.

[35] M. Lee, W. Lee, S. Choi, J. W. Jo, J. Kim, S. K. Park, Y. H. Kim, *Adv. Mater.* **2017**, *29*, 1700951.

[36] P. Stoliar, J. Tranchant, B. Corraze, E. Janod, M. P. Besland, F. Tesler, M. Rozenberg, L. Cario, *Adv. Funct. Mater.* **2017**, *27*, 1604740.

[37] J. C. Magee, *Nat. Rev. Neurosci.* **2000**, *1*, 181.

[38] A. Polsky, B. W. Mel, J. Schiller, *Nat. Neurosci.* **2004**, *7*, 621.

[39] A. R. Mehryar Mohri, Ameet Talwalkar, *Foundations of Machine Learning*, The MIT Press, Cambridge, US **2012**.

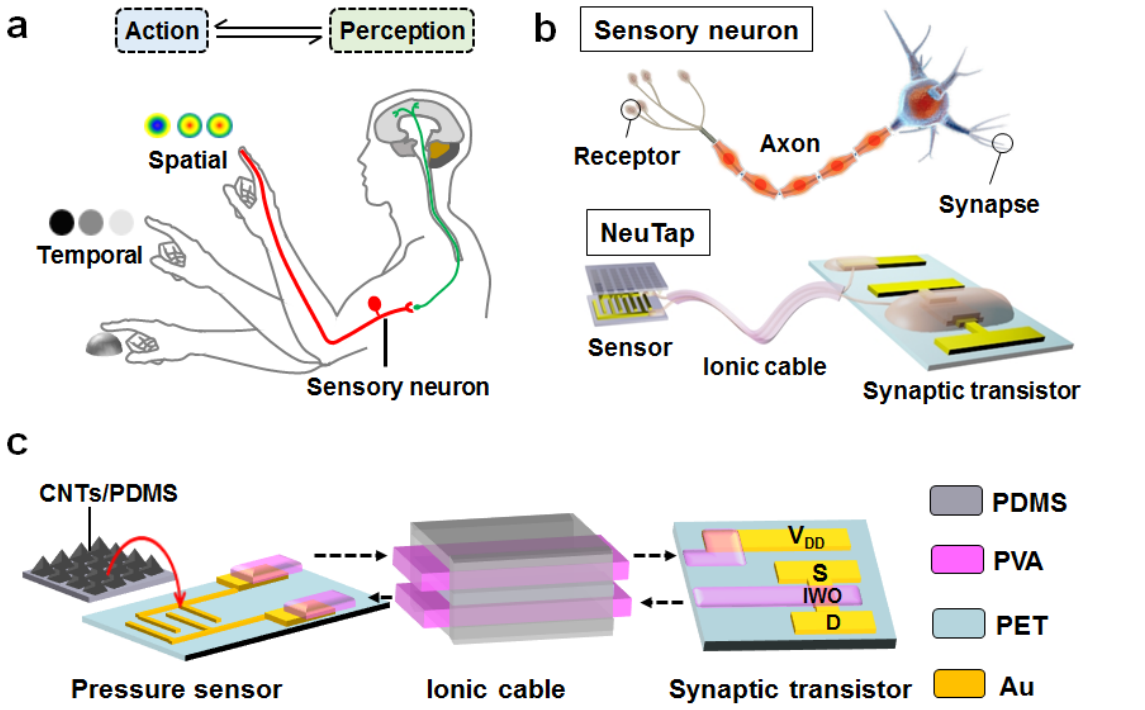

Figure 1. The concept design of NeuTap. a) Schematic illustrating the integration of the spatial and temporal features of a pattern by the tactile sensory neuron in an action-perception loop. **b)** A sensory neuron (top) compared to our NeuTap (bottom). **c)** Diagram illustrating the details of the NeuTap.

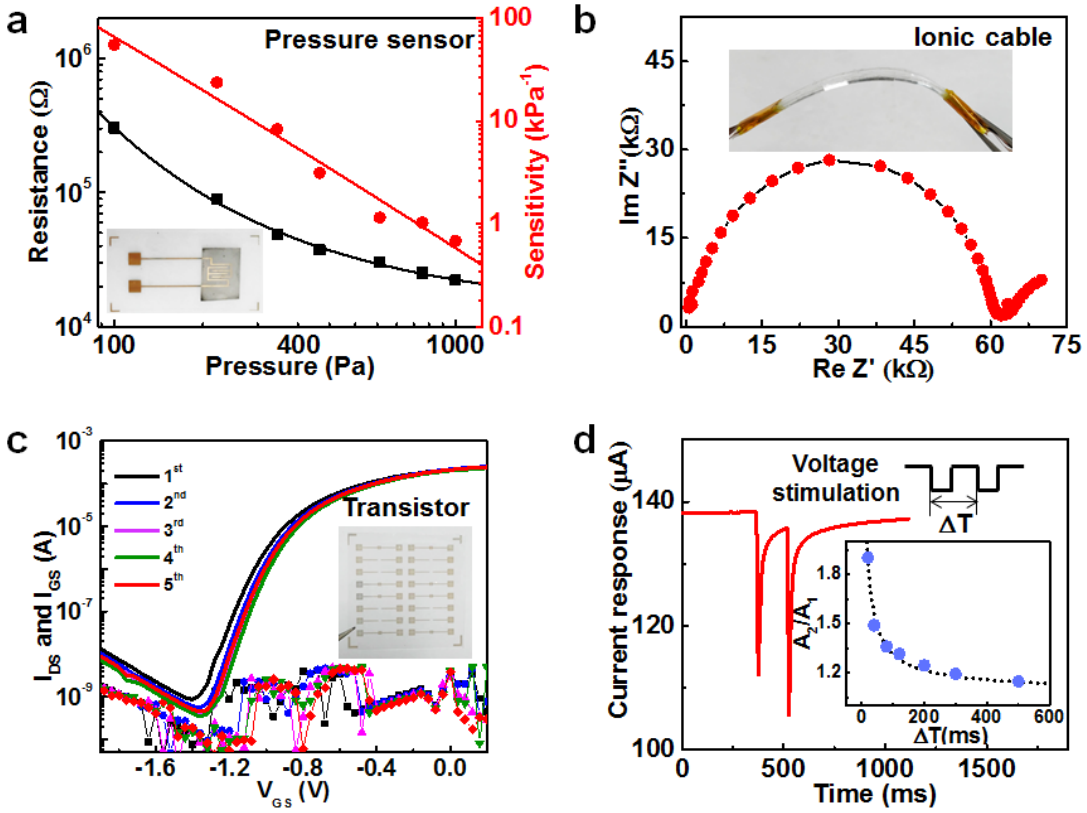

Figure 2. The electrical characterizations of NeuTap. a) Graph shows resistance and sensitivity change when different pressures are applied on the sensor. Inset: digital image of the pressure sensor. **b)** Cole-Cole plot of the PVA layer shows a perfect semi-circle. Inset: digital image of an ionic cable. **c)** Plot showing the transfer characteristics of the PVA gated IWO transistor with V_{DS}=1.5 V for 5 times. Inset: digital image of the transistors on PET substrate. **d)** PPF emulation by the synaptic transistors show two current peaks when two successive voltage pulses (-1.5 V, 10 ms) with a time interval (ΔT) of 200 ms are applied on the gate. Inset: Plot of the ratio between the two current peaks as a function of time interval (ΔT: from 20 to 500 ms).

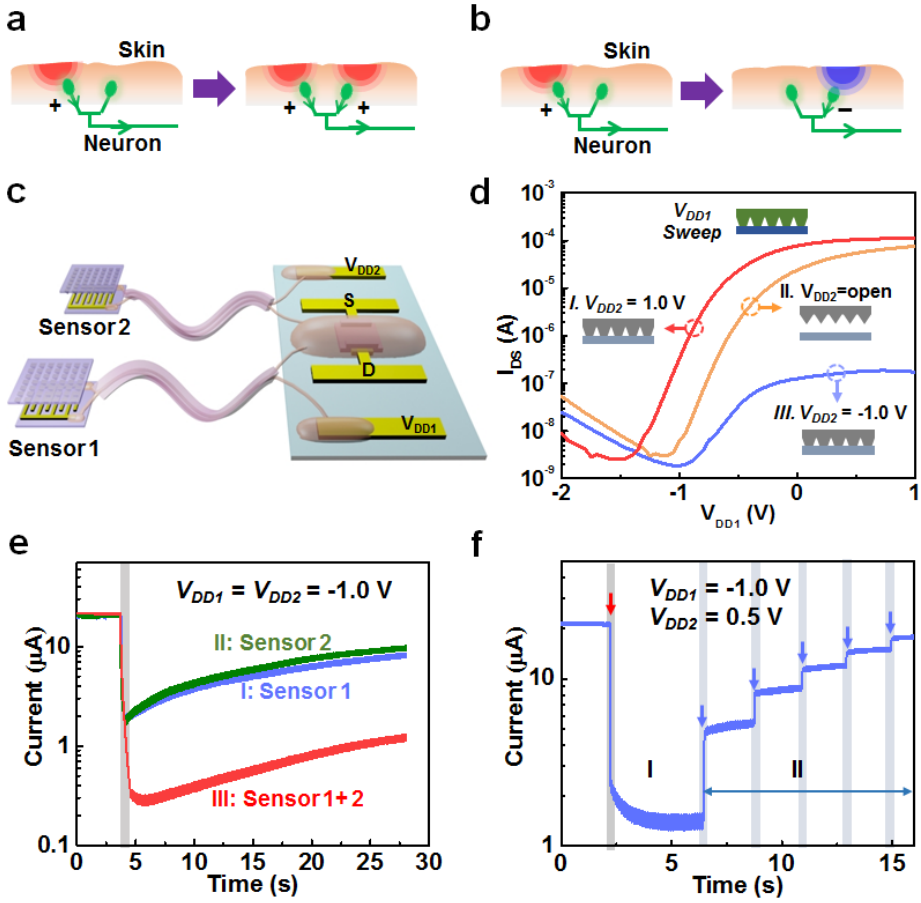

Figure 3. The spatiotemporal correlated stimuli integration by the NeuTap. Schematic diagrams showing the integration of two spatially isolated stimuli: **a)** Two stimuli (red circles) could excite the sensory neuron and augment the neuronal response; **b)** One stimulus could excite (red circles) while the other could inhibit (blue circles) the sensory neuron, accelerating the recovery from the first stimulation. **c)** Diagram illustrating the configuration of the NeuTap neuron with two pressure sensors. **d)** Plot showing the modulation effect of sensor2 on transfer curves of the IWO transistor with V_{DD1} voltage sweep. **e)** Plot showing current responses with V_{DD1}=V_{DD2}-1.0 V when sensor 1 and sensor 2 are pressed individually (case I and II), and when both sensors are pressed simultaneously (case III). **f)** The current integration by the two sensors with V_{DD1}=-1.0 V and V_{DD2}=0.5 V. Case I: triggered by a finger touch on sensor 1 at the beginning (red arrow). Case II: triggered by 5 finger touches on sensor 2 (blue arrows). Grey areas represent the touch action in all the cases, and the currents were measured with V_{DS}=1.5 V.

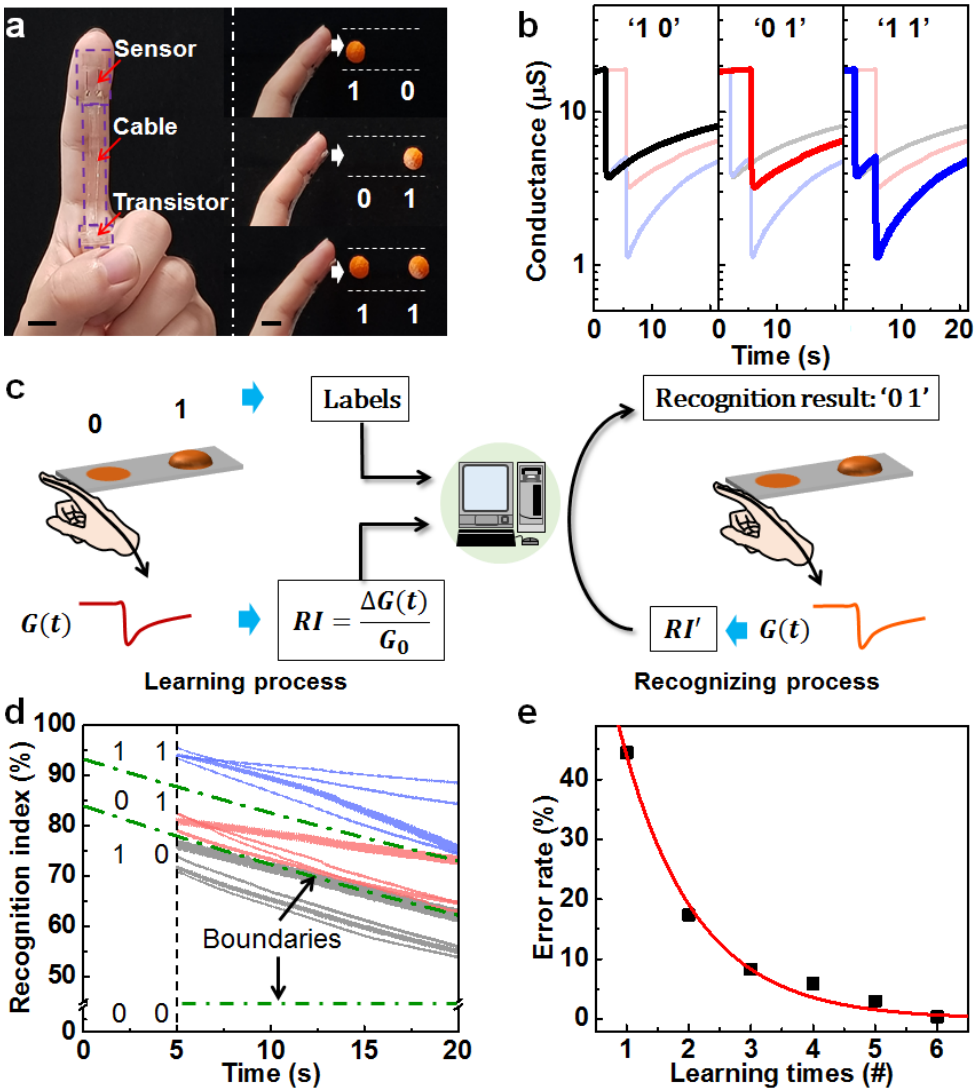

Figure 4. Tactile pattern recognition and perceptual learning by the NeuTap. a) Digital image showing the NeuTap on a finger (left) and schematic diagrams illustrating the pattern pairs and their corresponding two-bit binary code labels (right). The scale bar is 1 cm. **b)** Plot showing the typical responses of the NeuTap to three types of pattern pairs. The light shade curves are the other two types as a comparison. The conductance was measured with V_{DD}=-1.0 V. **c)** Schematic diagram illustrating the machine learning method for perceptual learning emulation. **d)** Plot shows the RI for four groups of training data. Each pattern pair is shown by light coloured lines. Green dash dot lines represent label boundaries. Pattern '00' is defined by RI<10%. **e)** The error rate of recognition plotted as a function of the learning times. The black squares are the measured data and the red line is the fitting curve.

The table of contents entry: A neuromorphic tactile processing system is built to mimic biological sensory neuron with sensing, refining, and learning. The spatiotemporal correlated tactile stimuli could be detected and integrated for pattern recognition. The recognition capability could be further enhanced by implementing perceptual learning processes. Such system would endow robots and prosthesis with artificial intelligence to extend their cognition and adaptability.

Keyword: artificial neuron, perceptual learning, artificial intelligence, electronic skin, neuromorphic engineering

Changjin Wan, Geng Chen, Yangming Fu, Ming Wang, Naoji Matsuhisa, Shaowu Pan, Liang Pan, Hui Yang, Qing Wan, Liqiang Zhu,* & Xiaodong Chen*

An Artificial Sensory Neuron with Tactile Perceptual Learning

ToC figure